



Growth mechanism of icosahedral and other five-fold symmetric diamond crystals

Qiu-ping WEI^{1,2,3}, Li MA^{2,3}, Jun YE⁴, Zhi-ming YU¹

1. School of Materials Science and Engineering, Central South University, Changsha 410083, China;

2. State Key Laboratory of Powder Metallurgy, Central South University, Changsha 410083, China;

3. School of Metallurgy and Environment, Central South University, Changsha 410083, China;

4. School of Materials Science and Engineering, Nanyang Technological University, Singapore 639798, Singapore

Received 28 February 2014; accepted 3 December 2014

Abstract: Five-fold symmetric diamond crystals (FSDCs) were synthesized by hot filament chemical vapour deposition (HFCVD) methods. Their surface morphologies and defects were characterised by scanning electron microscopy (SEM). From the perspective of nucleation-growth, a growth mechanism for icosahedral and other five-fold symmetric diamond crystals was discussed. Computer modelling was also carried out. The results show that the dodecahedrane ($C_{20}H_{20}$) molecule is proposed as a nucleus for the growth of icosahedral diamond crystals (IDCs), wherein the 20 $\{111\}$ surface planes develop orthogonal to the direction of the original 20 C—H bonds by sequential H abstraction and CH_3 addition reactions. IDC can be pictured as an assembly of isosceles tetrahedra, with each tetrahedron contributing a $\{111\}$ plane to the surface of the IDC and the remainder of the tetrahedral surfaces forming twin planes with neighbouring tetrahedra. The small mismatch (1.44°) between the $\{111\}$ surface dihedral angle of a perfect icosahedron and that of a twinned icosahedron reveals itself via twin planes in the IDC grain. The modelling suggests how the relief of strain induced by this distortion could lead to the formation of defects such as concave pentagonal cavities at vertices and grooves along the grain edges that accord well with those observed experimentally. Similar arguments based on growth from the hexacyclo pentadecane ($C_{15}H_{20}$) nucleus can also account for the observed formation of star and rod shaped FSDCs, and some of their more obvious morphological defects.

Key words: diamond; five-fold symmetry; icosahedron; dodecahedrane; defect

1 Introduction

The Platonic solids, comprising geometrically regular convex polyhedra, have been known since antiquity [1]. The faces of any Platonic solid are congruent regular polygons, with the same number of faces meeting at each vertex, thereby rendering their edges, vertices and angles congruent. There are just five Platonic solids: the tetrahedron, cube, octahedron, dodecahedron and icosahedron [1,2]. Classical theories of crystal structure allow only 2-, 3-, 4-, and 6-fold rotational symmetries, consistent with the ubiquity of tetrahedral, cubic and octahedral morphologies in naturally occurring crystals. Dodecahedra and icosahedra exhibit 5-fold rotational symmetry, however, which do

not appear in conventional crystals but have been observed (via diffraction studies) in materials termed quasicrystals [3]. Since the discovery of systems with icosahedral point group symmetry [4], the concept of quasicrystals led the International Union of Crystallography to redefine the term crystal to mean “any solid having an essentially discrete diffraction diagram” [5], thereby shifting the essential attribute of crystallinity from position space to Fourier space. Quasicrystals display long-range order but belong to non-crystallographic point groups (including 5-, 8-, 10- or 12-fold rotation axes), and form patterns that fill space without formation of a conventional lattice (due to the lack of translational symmetry) [6]. Numerous quasicrystals have been reported, and confirmed, since the original discovery by SHECHTMAN et al [7].

Foundation item: Projects (51301211, 21271188) supported by the National Natural Science Foundation of China; Project (2012M521540) supported by the China Postdoctoral Science Foundation; Project (2013RS4027) supported by the Postdoctoral Science Foundation of Hunan Province, China; Project (20110933K) supported by the Open Foundation of the State Key Laboratory of Powder Metallurgy, China; Project supported by the Open-End Fund for Valuable and Precision Instruments of Central South University, China

Corresponding author: Li MA; Tel: +86-731-88830335; Fax: +86-731-88876692; E-mail: marycsupm@csu.edu.cn

DOI: 10.1016/S1003-6326(15)63762-1

Many quasicrystals are found to be associated with face-centred cubic systems, especially in aluminium alloys (Al–Li–Cu, Al–Mn–Si, Al–Ni–Co, Al–Pd–Mn, Al–Cu–Fe, Al–Cu–V), but many other compositions (Cd–Yb, Ti–Zr–Ni, Zn–Mg–Ho, Zn–Mg–Sc, In–Ag–Yb, Pd–U–Si) are also known [8]. Quasicrystals typically display high hardness, low thermal conductivity and low friction, and exhibit remarkable electronic (such as strongly anisotropic electronic transport) [9] and photonic bandgap properties [10].

Many families of icosahedral quasicrystals have received widespread attention in recent years [11–15], including carbon-based systems [16–18]. Icosahedral morphologies are often observed in diamond crystals grown by chemical vapour deposition (CVD) methods [19–21], and many of these icosahedral diamond crystals (IDCs) show characteristic morphological defects (dimples at the vertices, or grooves between abutting faces) [22]. IDCs are often seen in short duration CVD experiments before the individual crystallites emerging from different nucleation sites grow sufficiently to form a continuous polycrystalline film. Several reports have addressed aspects of the formation mechanism, atomic structure and defects of icosahedral carbon clusters and IDCs [16–19,22–24]. The formation of IDCs with five-fold symmetry has been explained in terms of three stacking errors during growth on different {111} surfaces [23], but MATSUMOTO and MATSUI [19] advanced a “molecular” based mechanism wherein caged hydrocarbons like dodecahedrane ($C_{20}H_{20}$) and hexacyclo pentadecane ($C_{15}H_{20}$) might act as nuclei (“embryos”) for the growth of IDCs and rod shaped five-fold symmetric diamond crystals (FSDCs), respectively. The present work explores the latter proposal further. Specifically, it reports the synthesis of IDCs and other FSDCs by hot filament (HF) CVD methods, the characterization of their surface morphologies and defects by scanning electron microscopy (SEM), and the companion computer modelling. The computer modelling provides strong support for the view that caged hydrocarbon molecules are indeed very plausible nuclei for the subsequent growth of IDCs and other FSDCs in an HFCVD environment.

2 Experimental

Diamond crystals were grown in an HFCVD reactor, as described previously [25]. Si(100), Si(111), tungsten (99.999% purity), WC–Co (13%, mass fraction) and carbon steel with a high velocity oxy-fuel (HVOF) sprayed WC–Co coating were all used as substrates to grow IDCs and FSDCs. No nucleation enhancing

techniques (scratching or ultrasonic agitation with diamond dust) were used for any of the substrates. While it is straightforward to achieve a low diamond nucleation density on the polished single crystal silicon, a prerequisite for formation of isolated crystallites rather than a continuous thin film. This substrate is not well suited for subsequent SEM imaging of small diamond crystals which were deposited on its surface. Successful FSDC formation is sensitive to the choice of substrate and the CVD process condition [26]. High purity tungsten substrate is proved to be the choice of substrate for the growth of FSDCs for subsequent analysis. To reduce the nucleation density, a thin film of tungsten (purity 99.999%) was deposited on the surface of these substrates by magnetron sputtering prior to diamond deposition. Deposition time, H_2/CH_4 ratio, nucleation density and substrate temperature were varied in order both to optimise the formation of FSDCs (rather than alternative crystallite morphologies), and to form FSDCs with a range of morphologies and sizes. Figure 1(a) shows the plan view SEM images, and Fig. 1(b) shows the SEM image taken at an oblique viewing angle and the cross-sectional image of the FSDCs growing from the substrate surface. WC–Co (13%, mass fraction) and carbon steel (with a HVOF sprayed WC–Co interlayer) substrates were used to grow denser films containing a high IDC fraction. Figure 1(c) shows an SEM image of such a film. The type of substrate used and the deposition

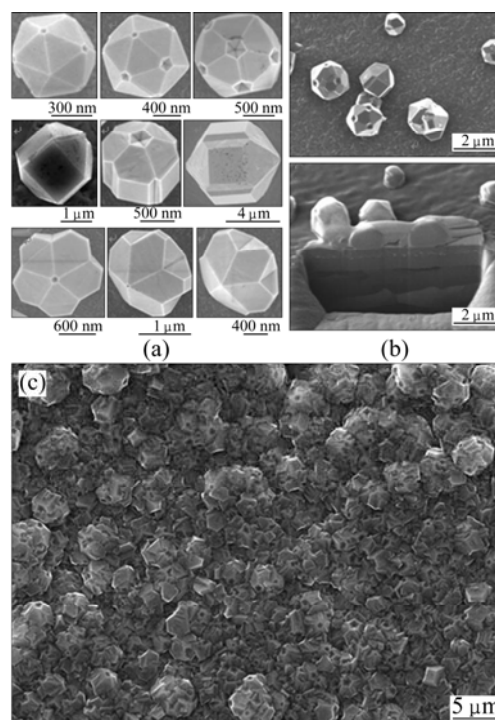


Fig. 1 Plan (a) and glancing angle cross-sectional (b) SEM images of individual IDC and FSDCs, and SEM image of polycrystalline diamond film with high IDC density (c)

conditions are not discussed in the following analysis in relation to any particular grain or defect morphology.

3 Growth model for icosahedral diamond crystals

3.1 Preamble

The surface free energy (γ_{hkl}) of the (hkl) face of diamond is given by

$$\gamma_{hkl} = \frac{\lambda}{\sqrt{h^2 + k^2 + l^2}} \frac{3E}{8d_0^2} \quad (1)$$

where E and d_0 are the C—C bond energy and bond length in diamond, respectively, and λ represents the maximum value of the Miller indices, h , k and l [27]. Equation (1) shows the anisotropy of the surface free energy of different diamond planes and gives rise to the relationship

$$\gamma_{100} : \gamma_{110} : \gamma_{111} = 1 : \frac{1}{\sqrt{2}} : \frac{1}{\sqrt{3}}$$

Clearly, the (111) surface of a diamond crystal has the minimum surface free energy [30]. It has long been recognised that the surface free energy plays a critical role in determining the equilibrium morphology of a crystal. Gibbs showed that a given crystal volume will be in equilibrium with its surroundings when its total surface free energy G is a minimum, i.e.,

$$G = \sum_{(100)}^{hkl} \gamma_{hkl} A_{hkl} \rightarrow \text{minimum} \quad (2)$$

where A_{hkl} is the area of the (hkl) face [28]. The equilibrium shape of diamond is thus an octahedral crystal with eight (111) surfaces because this has the lowest total surface energy for a given volume. The surface area of an icosahedron is actually ~10% smaller than that of an octahedron with the same volume (Table 1). Thus the Gibbs condition for crystal growth would be fulfilled more efficiently if the diamond crystal has the shape of an icosahedron, because each surface is a (111) facet, i.e., $\sum \gamma_{hkl} A_{hkl}$ is minimized. Thus, as long as the appropriate growth nucleus exists and the mechanistic growth conditions are satisfied, a diamond crystal might be expected to grow into an icosahedron.

Table 1 Properties of Platonic solids

Platonic solid	Surface Area (A)	Volume (V)	k
Tetrahedron	$\sqrt{3}a^2$	$\sqrt{2}a^3/12$	7.21
Cube	$6a^2$	a^3	6.00
Octahedron	$2\sqrt{3}a^2$	$\sqrt{2}a^3/3$	5.72
Dodecahedron	$3\sqrt{25+10\sqrt{5}}a^2$	$(15+7\sqrt{5})a^3/4$	5.31
Icosahedron	$5\sqrt{3}a^2$	$5(3+\sqrt{5})a^3/12$	5.15
Sphere	$4\pi r^2$	$4\pi r^3/3$	4.84

a is the edge length and k is the surface area per unit volume

The following discussion focuses on IDCs but, as shown later (Section 4), similar arguments hold for other FSDCs. SCHULMAN et al [29] discussed the dodecahedrane molecule from the viewpoint of group theory, graph theory and molecular orbital theory prior to its synthesis and characterization by PAQUETTE et al [30–34]. As shown in Fig. 2, the C—C bonds in dodecahedrane form the edges of pentagons and meet at (exterior) $\angle C-C-C$ bond angle $\sim 108^\circ$ (as required for dodecahedral symmetry), while the $\angle H-C-C$ bond angle is calculated to be $110^\circ 54'$, which is very close to the $109^\circ 28'$ value characteristic of an idealised tetrahedral (sp^3) structure. As a result, dodecahedrane is almost devoid of angle strain. The C—C framework bond lengths are in the range of 1.535–1.541 Å, essentially identical to that in bulk diamond.

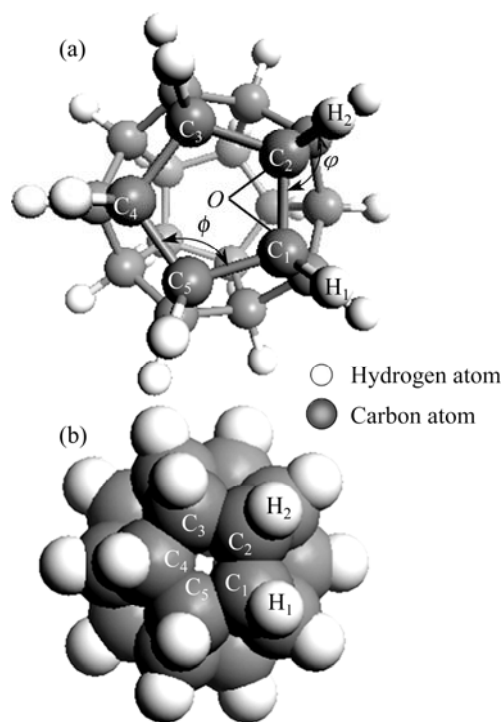


Fig. 2 Dodecahedrane molecule shown as ball-stick model (a) and space filling model (b)

Dodecahedra and icosahedra both have the same 5-fold rotational symmetry so, geometrically at least, the transition from a dodecahedral nucleus to an icosahedral quasicrystal should be possible. The C—H bonds in dodecahedrane approximate those on a (111) face of an sp^3 hybridized diamond crystal. Diamond growth by CVD from activated hydrocarbon/ H_2 gas mixtures involves the breaking of surface C—H bonds (by H atom abstraction reactions) and the formation of new C—C bonds (typically by the addition of CH_3 radicals to the resulting surface radical sites) [35]. In the limit that CH_3 groups replace all the H atoms in dodecahedrane, an embryonic (111) plane will develop orthogonal to each of

the original C—H bonds. Continued substitution of surface H atoms by CH₃ radicals would lead to the emergence of an icosahedral crystal bounded by 20 {111} planes—an IDC, as illustrated in Fig. 3.

A perfect icosahedron can be pictured in terms of twenty identical isosceles tetrahedra (Fig. 4). The distance from the centre of an icosahedron to the outer surface (Oh_1 or Oh_2 in Fig. 4) is 7.44% shorter than that in a regular tetrahedron. Each tetrahedron thus has three isosceles faces ($\triangle OAB$, $\triangle OBC$ and $\triangle OAC$) and one regular ($\triangle ABC$) triangular face (Fig. 4(a)). The former are located at the interfaces with neighbouring tetrahedra, while the latter contributes to the surface of the icosahedron. Thus an icosahedron can be described in terms of 30 isosceles triangular interfaces and 20 regular triangular surfaces, with a dihedral angle, $\angle h_1mh_2 = \alpha_{(111)} = 138.19^\circ$ (Fig. 4(b)).

Now considering diamond. The surfaces of small, regular tetrahedral diamond grains are typically the triangular {111} planes. The interface (OAC) between two tetrahedral grains in contact must be a twinning plane, with dihedral angle $\angle h_1mh_2 = \theta_{(111)} = 141.06^\circ$ in Fig. 5(a). The corresponding bond structure of the topologically close-packed (TCP) grain is shown in Fig. 5(b). The interface between two tetrahedral grains is similar, but not identical, to that between two isosceles

tetrahedra that make up an icosahedron. The regular tetrahedron is actually one of the simplest shapes for which the packing of Euclidean space is problematic. Dense, ordered structures become possible, however, extra space is allowed between the tetrahedra. In the limit of infinite pressure, an arrangement with maximum packing fraction is stable because it minimizes the specific volume and Gibbs free energy [36].

3.2 Distorted twin planes

It has been seen that the dihedral angle $\theta_{(111)}$ associated with the twin plane in the TCP diamond crystal is 141.06° . However, the dihedral angle $\alpha_{(111)}$ in a regular icosahedron is 138.19° . Therefore, a TCP crystal cannot develop to an icosahedral grain simply by normal twinning. Some lattice mismatch is required if the TCP crystal is going to form a regular icosahedral grain. Specifically, an extended network based on C—C bonds and sp^3 coordinated atoms can only form, when some distortion across the twin boundaries of the IDC allowed. To minimize strain in the crystal structure, the lattice mismatch arising from the difference in dihedral angles will be focused on the 30 twin planes of the icosahedron, and the twin plane will become a distorted twin plane (DTP). The structure of the DTP is illustrated in Fig. 6, which highlights the fact that the C—C bonds across the

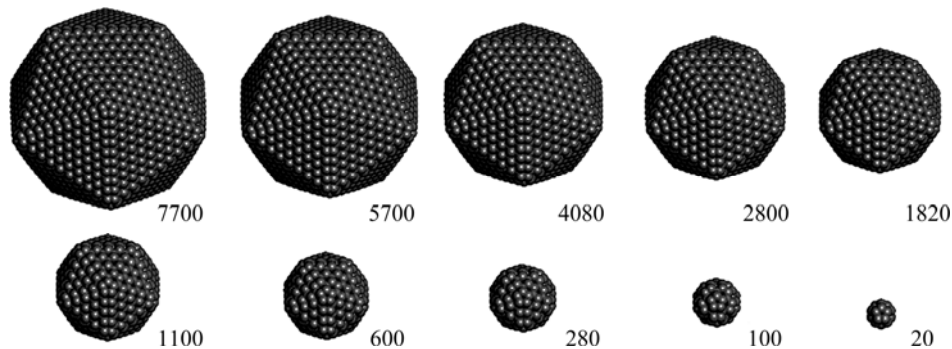


Fig. 3 Schematic illustration of evolution of $C_{20}H_{20}$ nucleus into IDC model by layer-by-layer replacement of surface H atoms by C atoms

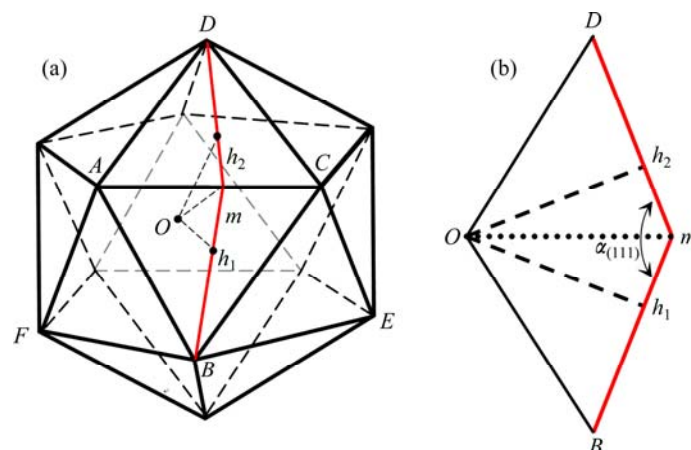


Fig. 4 Diagram illustrating icosahedron consisting of 20 isosceles tetrahedra with $Oh_1 = Oh_2$ (a) and $OBmD$ face (b)

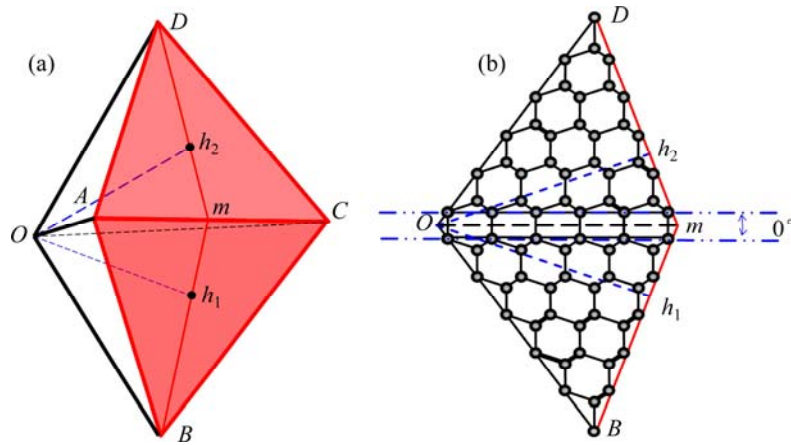


Fig. 5 Schematic of topologically close-packed twin (a) and cross-section illustrating bond structure at TCP twin boundary (b)

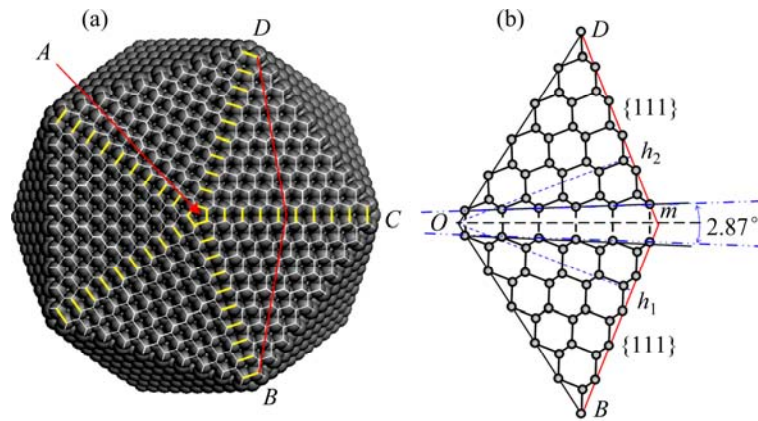


Fig. 6 IDC model consisting of 7700 carbon atoms produced using Materials Studio® modeling program (a) and crystalline structure of {111} distorted twin plane in IDC (line Om bisects DTP) (b)

DTP must be slightly stretched or bent in order to preserve icosahedral symmetry.

Micron-sized particles contain tens of thousands of atoms. Ab-initio calculations of such particles are generally prohibitive. Thus a less computer intensive approach, the classical force-field method was adopted, with the aim of gaining a qualitative understanding of the properties of IDCs. The Dreiding force-field is widely used to study carbon based materials like graphite. It can also describe the conventional diamond structure (i.e., sp^3 C—C bonds and C—H surface bonds) well, and form a good starting point for obtaining reliable optimized structures and total energies of the IDCs of current interest. The geometries of all particle structures considered here were optimized using the following convergence criteria: total energy was smaller than 2×10^{-5} kJ/mol, interatomic interaction strength was smaller than 0.001 kJ/(mol·Å) and displacement was smaller than 1×10^{-5} Å. The number of iterations was set sufficiently large to guarantee the convergence of each calculation.

To model the bonding structure of IDCs, grains with increasing number of C atoms, ranging from 20 to 7700,

are investigated, as illustrated in Fig. 3. Successive IDCs in this series are formed by surrounding the previous one with another complete shell of C atoms. The IDC surface in each case was hydrogen terminated to stabilize the outermost layer of carbon atoms. In this regard, the surface of the model cluster is directly analogous to the growing surface of a diamond film during CVD from hydrocarbon/ H_2 gas mixtures. The number of C atoms, n , in the different shells of a defect-free IDC grain is given by

$$n = 20 \sum_{k=0}^{N^*} (k+1)^2 \quad (3)$$

where k is the shell number. Figure 7 shows the calculated variation in the C—C bond length in the pentagons perpendicular to the OA axis of a defect-free IDC (see Fig. 6) as a function of distance R_{OA} from the origin, O . This calculation reproduces the bond length of 1.54 Å in the 20 atom cluster (dodecahedrane, $k = 0$), and highlights the progressive compression of the C—C bond lengths in the pentagons at small R_{OA} in the larger clusters.

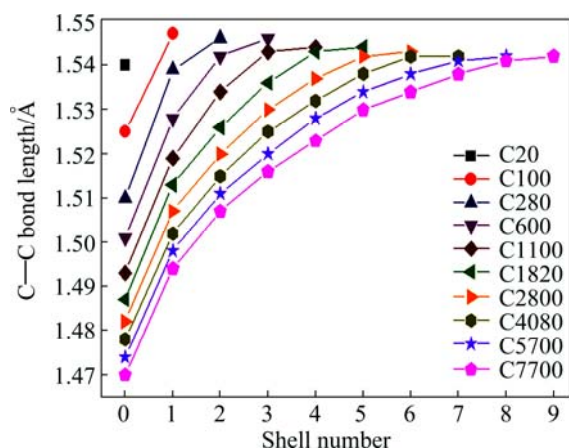


Fig. 7 Calculated variation in C—C bond lengths bridging DTP between neighbouring $\{111\}$ sectors

To explore the change in C—C bond length at the twinning interfaces, the largest (7700 carbon atoms) IDC is investigated. The surface of the IDC was again H-terminated to stabilize the outermost layer, and the bond length at the twinning interface was determined following geometry optimization. Figure 8 shows the calculated variation in C—C bond length across the triangular interface of the DTP (across ΔOAC in Fig. 6) for each of the 10 shells ($0 \leq k \leq 9$). The C—C bonds at the DTP are clearly compressed in the core, but stretched at the surface. As shown in Fig. 8, the C—C bond length varies symmetrically across the isosceles triangular DTP. Noting that hydrogen termination at the IDC surface relaxes the strain across the DTP and thus lowers the calculated C—C bond length in the outermost shell. This is true for any surface bonds and should be ignored.

The total energy of different sizes of defect-free IDC was calculated both with and without H-termination of the surface atoms. Figure 9 shows the calculated total

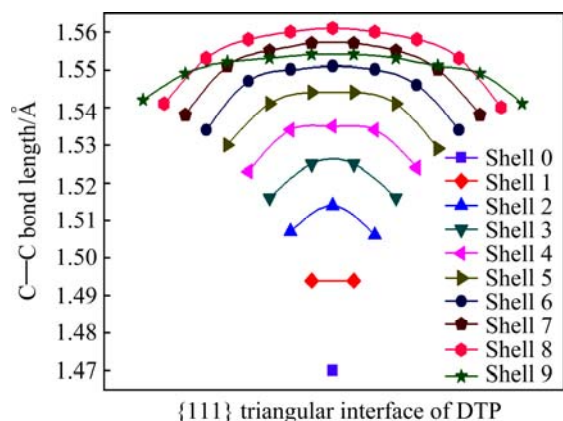


Fig. 8 Variation of C—C bond length across $\{111\}_{IT}$ DTPs in IDC consisting of 7700 carbon atoms produced using Materials Studio® modeling program (x axis indicates approximate position of C—C bond relative to triangular DTP plane ΔOAC in Fig. 6)

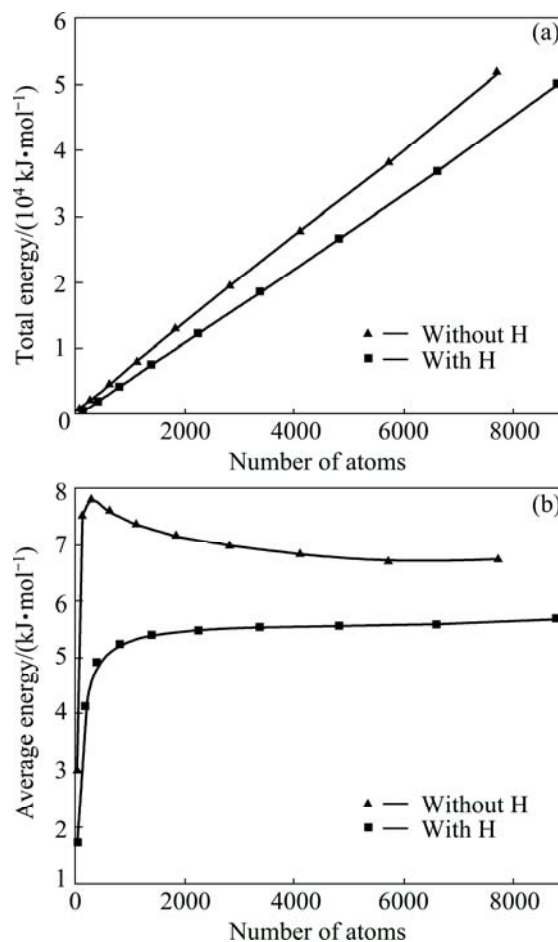


Fig. 9 Total energy (a) and average energy per atom (b) calculated for IDCs model with and without H-termination, as functions of total number of atoms

energy and the average energy per C atom, as function of the total number of atoms in the IDC. The total energy increases near linearly with the total number of atoms (Fig. 9(a)). The calculated total energy of the H-terminated IDC is less than that of the unterminated analogue (although the greater number of atoms in the former case), highlighting the importance of the surface terminating hydrogen atoms in reducing the surface energy of a bare icosahedral particle with its attendant dangling bonds. The average energy per atom plot (Fig. 9(b)) also serves to illustrate the energy stabilization caused by H-termination. It is noted that, in the H-terminated case, the average energy per atom increases slowly once the total number of atoms exceeds ~ 1000 , while in the unterminated case, the average energy per atom falls abruptly in the case of the smallest IDCs. The latter situation is more likely due to the stress generated from the bond distortion as the size of icosahedral particles increases. Therefore, the internal stress can, to some extent, be relieved by H-terminating the dangling bonds at the surface of the particles. Is this a fair comparison, since you are counting the surface H

atoms in the total number of atom count?

In the comparison of average energy, it is meaningless to compare the absolute value due to the force-field description of C—H bond, which is impossible for one to distinguish the specific contributions of valence energy from C or H atoms. However, it is clear that C and H atoms should have large difference in contributing to the valence energy terms, thus the trend of average energy is still meaningful in illustrating the role of H-termination in relieving the stress associate to the dangling bonds of surface C atoms.

Comparing the total energy (or the average energy per atom) calculated for the H-terminated and unterminated particles suggests a plausible role for hydrogen in determining the growth morphology of icosahedral particles, especially at the very early stages of the growth process (for particles consisting of less than 1000 carbon atoms). Without H-termination of the surface atoms, an embryonic icosahedral particle consisting of 280 C atoms will involve large internal stresses due to the distortion of the C—C bonds. Such behavior hints at likely instability in the early growth stage, which may encourage alternative morphologies or defects which map through into alternative eventual particle shapes, as observed in the SEM images.

3.3 Defects and dimples

Structural defects consisting of 5-fold symmetric recesses or “dimples” located on the vertices and edges of diamond particles have been observed experimentally [22]. Figure 1(a) shows several examples of the wide variety of possible morphologies. Structures that closely resemble those observed experimentally can also be generated by the present model, simply by breaking some of the C—C bonds between the 20 tetrahedra that make up the IDC. Other types of defect are also found experimentally, but this type of defect is concerned here as it appears to be induced by bond dislocations at the DTP. Thus breaking different numbers of bonds is investigated (defined by the number of shells penetrated by the defect, starting from the IDC surface, as shown in Fig. 10), which will have the effect of relieving strain across the DTP. The terminology is defined with reference to the 7700 atoms IDC particle, in which nine shells separate the surface from the central C₂₀ nucleus. A level 1 defect is defined as one that involves breaking bonds in the outermost shell only (i.e., shell 9 in Fig. 10), while a level 8 defect in this case would involve breaking bonds in the DTP all the way from the exterior through to shell $k=2$. The resulting structures were optimized with the same convergence criteria as used when optimizing the geometries of the perfect structures.

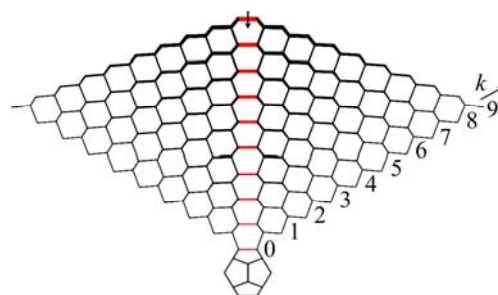


Fig. 10 Diagram illustrating defect formation by cleaving selected bonds (shown in red) along DTP in IDC model consisting of 7700 carbon atoms (The number of bonds per layer that need to be broken to form defect along DTP decreases towards nucleus)

Breaking selected bonds across the DTP allows geometry optimization for a range of defect exhibiting particles, and comparison of their total energy (and the average energy per atom) as functions of defect level, i.e., the depth to which the defect penetrates towards the core. This, in turn, can provide insights into the effect of internal stress originating from bond distortion during IDC growth. Figure 11 shows the results for bare IDCs with $3 \leq k \leq 9$, as functions of defect level. Each IDC displays a similar trend, wherein the highest energy situation is obtained by breaking bonds down to the second or third shell from the outer surface. The calculations also predict that the total energy drops to a minimum when the defect propagates from the first ($k=0$) shell, i.e., when the C₂₀ core is isolated from the rest of the structure. The total energy in this case is simply that of the 20 non-interacting tetrahedra plus that of the isolated C₂₀ core.

Figure 12 displays the optimized structures for IDCs based on 4080 carbon atoms (i.e., 7 shells outside the C₂₀ core), with defects ranging from level 1 to 7. The icosahedra (I_h) symmetry of these particles is clearly breaking down when the defect extends to level 5 (i.e., from the $k=2$ shell to the external surface). As shown in Fig. 11, the calculated total energy of these defective structures (and the average energy per atom) lies below that of the perfect IDC (i.e., below the “defect level 0” energy). Such observations hint at a possible formation mechanism for this type of defects during IDC particle growth. The strain on C—C bonds across the DTP must have an important role in determining the shape of the icosahedral particles. Within the present model, the intrinsic strain within a defect-free IDC increases as the particle grows from the initial C₂₀ nucleus. As shown in Fig. 11, this strain can be relieved by breaking bonds along the DTP, leading to the characteristic topological features (grooves between adjacent twin planes, and pentagonal voids at the vertices between 5 adjacent twin planes) illustrated in the computed minimum energy

structures (Fig. 12). Upon continuing growth, these embryonic defects will extrapolate into topological features (grooves between planes, and 5-fold symmetric dimples) as observed by SEM images of the micron sized

IDCs shown in Figs. 1 and 13. When the I_h symmetry of these particles has been broken down as shown in Figs. 12(Levels 6 and 7), if the diamond continues growing, the growth will be very similar with the

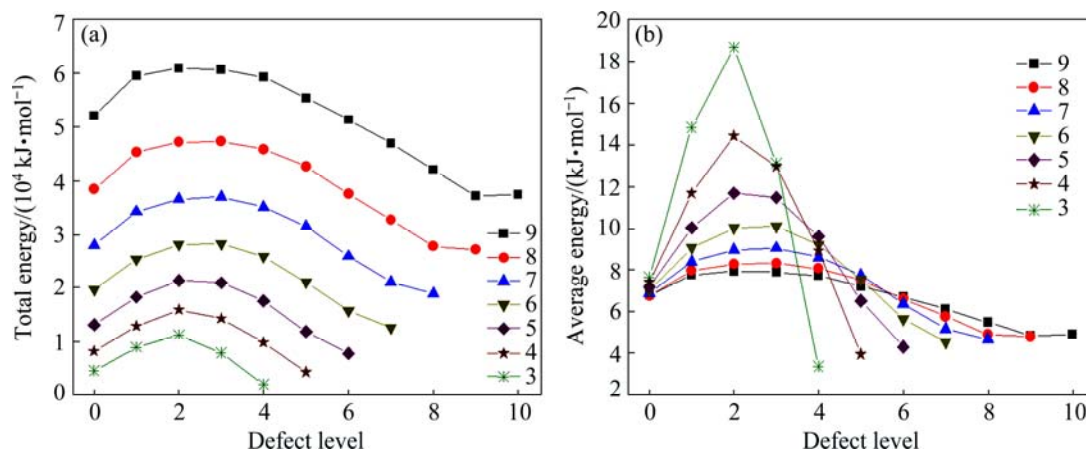


Fig. 11 Total energy (a) and average energy per atom (b) of defect exhibiting IDCs (without H-termination) as functions of defect propagation depth within IDC

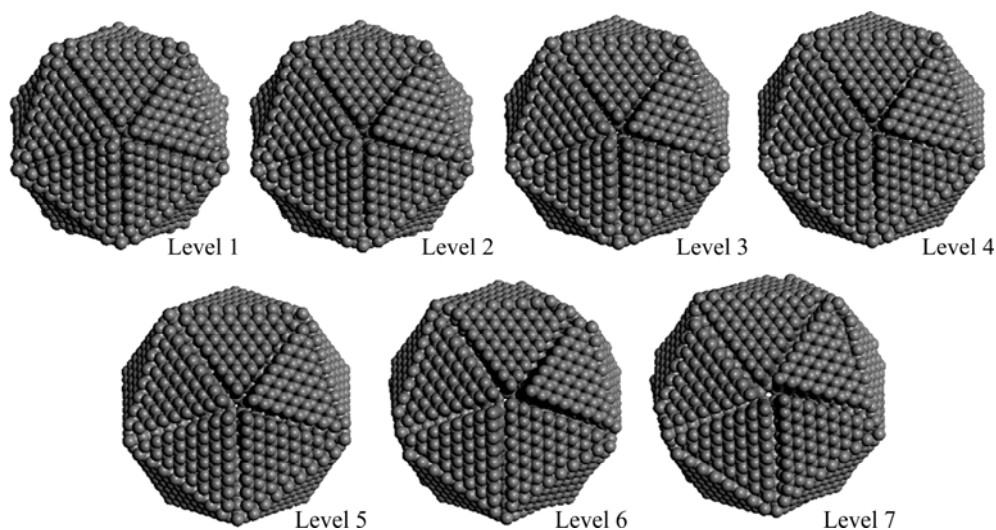


Fig. 12 Geometric evolution of IDC model consisting of 4080 C atoms with defects ranging from levels 1 to 7

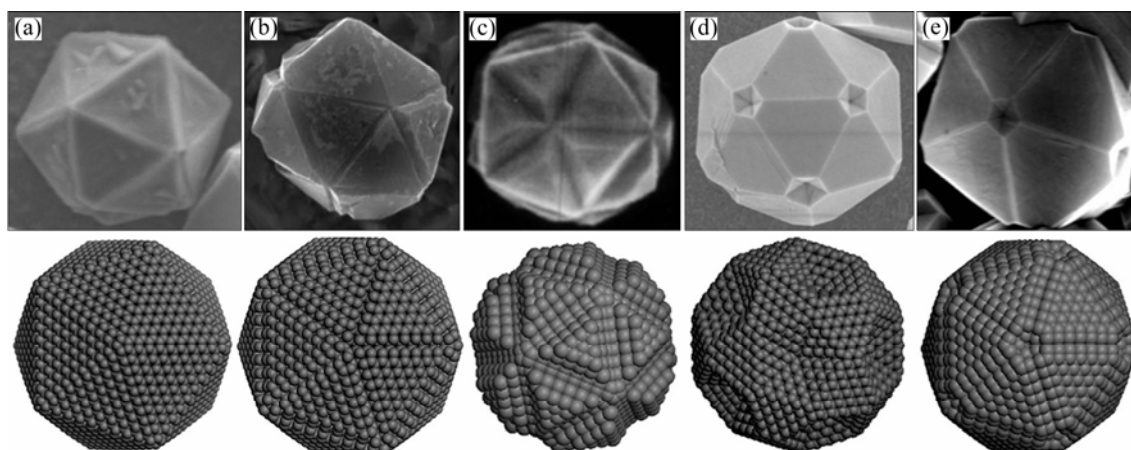


Fig. 13 CVD grown IDCs showing both perfect icosahedron (a) and a variety of defects (b–e) seen by SEM and modeled using Materials Studio® program (Fig. 13(c) replicated from Ref. [22])

isoepitaxial growth at the diamond (111) surface. Finally, the grown diamond crystals will not be able to form the perfect five-fold symmetry. Some (111) planes may grow faster than others, some (111) planes may grow overlap at the twin boundary. So, the FSDCs will lose their perfect five-fold symmetry easily due to the high stress of the DTP. This is the reason of many kinds of non-perfect FSDCs observed in the SEM images. But this does not deny the importance of the nucleus to form the FSDCs.

The DTP is a two-dimension defect which has a higher energy than the ideal twin plane. The strain across these distorted twin planes must be reduced during the growth process, for example, by the addition of extra carbon atoms into stretched bonds and producing the IDC structures shown in Fig. 12. The IDCs with defect occurring as “grooves” along the edges have lower surface areas than the defect-free IDCs with the same number of atoms. Therefore, the surface energy is not increased by the formation of this defect morphology.

4 Growth model for other five-fold symmetric diamond crystals

As noted previously [19], another caged hydrocarbon, hexacyclo pentadecane ($C_{15}H_{20}$), appears ideally suited to act as a nucleus for growing rod shaped FSDCs. As shown in Fig. 2, IDCs and both rod and star shaped FSDCs often appear together under the same CVD conditions. $C_{20}H_{20}$ is composed solely of 5-member rings, whereas $C_{15}H_{20}$ consists of two 5-member rings

linked by five bridging CH_2 groups (thereby forming five 6-member rings around the girth, as shown in Fig. 14(a)). The 10 carbon atoms associated with the two planar cyclopentane-like rings each link to other three C atoms and one H atom, and are thus very reminiscent of C atoms on the diamond (111) surface with a terminating C—H bond. The bridging C atoms, in contrast, bond to two C atoms and two H atoms, reminiscent of the (unreconstructed) H-terminated diamond (100) surface. With the IDC growth considered previously, it can envisage that this hydrocarbon nucleus grows by successive H abstractions and CH_3 radical additions. The $C_{15}H_{20}$ nucleus offers a great diversity of the final structures, however, since growth is along two different directions, $\langle 111 \rangle$ and $\langle 100 \rangle$, the relative rates of which can be influenced and controlled by changing the CVD conditions [37,38]. Figure 14(b) shows a partial growth structure, Fig. 14(c) illustrates the transformation from the molecular to the crystallographic frame, and Figs. 14(d) and (e) anticipate both rod and star shaped morphologies in the event that the growth rate is faster along the $\langle 100 \rangle$ and $\langle 111 \rangle$ axes, respectively. As in the case of the IDCs, the 5-fold symmetry of the FSDC is inextricably linked to the presence of the 5-member carbon ring(s) in the molecular template from which it is assumed to nucleate.

In the previous discussion of IDC growth, there is a small mismatch between the equilibrium bond angles (and lengths) in the template molecule and the classic sp^3 structure. The $\angle C-C-C$ bond angle in the 5-member ring is $\sim 108^\circ$, whereas the $\angle C-C-C$ bond angle in

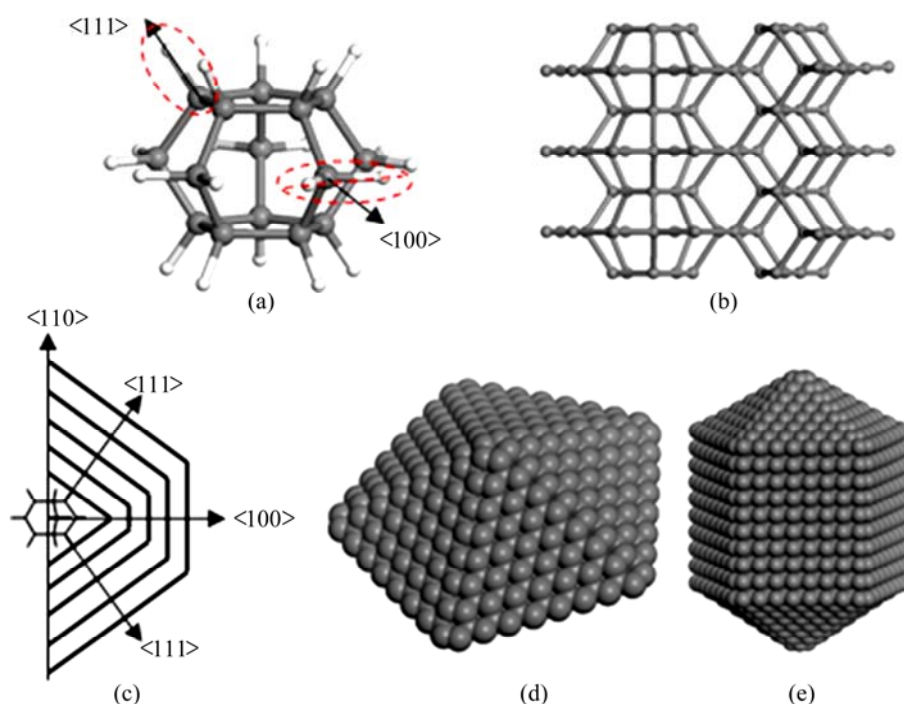


Fig. 14 $C_{15}H_{20}$ (a) and local structure of five-fold symmetric crystal growth from $C_{15}H_{20}$ (b), transform relationship of star-like and rod-like 5-fold symmetric diamond structures (c), calculated star-like FSD structure (d) and calculated rod-like FSD structure (e)

diamond is $109^{\circ}28'$. Therefore, there is an accumulation of strain in the C—C bonds at the (110) twin interface during growth of star and rod shaped FSDCs as a result of this $\sim 1^{\circ}28'$ mismatch (Fig. 15(a)). Such strain can again be released by the emergence of DTPs, resulting in the types of defect illustrated in the calculated minimum energy structures displayed in Figs. 15(b) and (c), which again are strikingly reminiscent of experimentally observed FSDC morphologies.

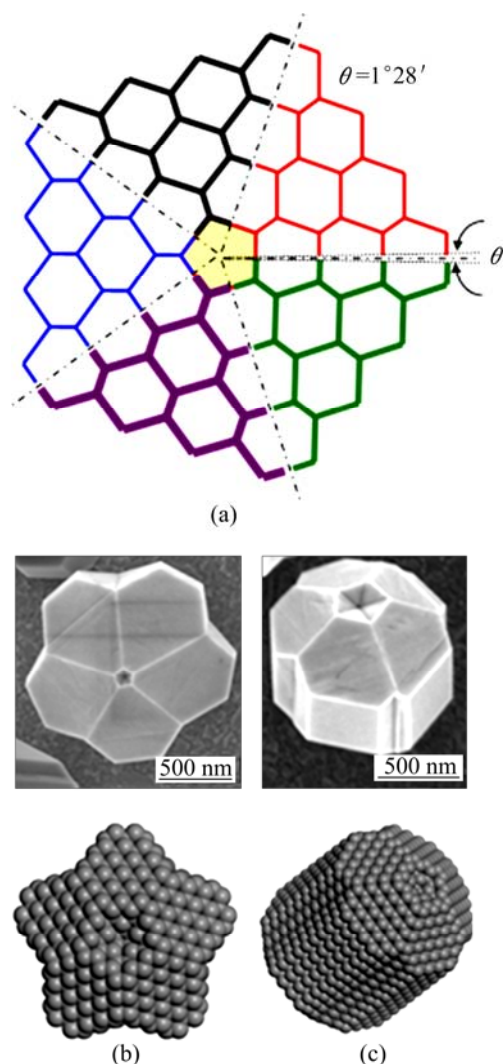


Fig. 15 (110) surface atomic structure of star- or rod-like five-fold symmetric center (a), and SEM images of star-like (b) and rod-like (c) FSDCs with model structures

5 Discussion

In concluding this study, it is important to recognise a number of caveats. The diameter of the largest particle modelled in this work (the 7700 C cluster) is only ~ 5 nm. Thus the largest model particles are still at least an order of magnitude smaller than the as-grown IDCs imaged in Fig. 1. BUHLER and PRIOR [22] have previously explored the development of individual IDCs during

CVD growth. Imaging constrains meant that they could only monitor the evolution of particles that had already grown to diameters greater than $0.25 \mu\text{m}$ but, in no case, did they observe a change in the principal crystal appearance during the subsequent growth. Thus they concluded that the morphology of a multi-ply twinned particle was established in the very early nucleation stage, entirely consistent with the present proposal that FSDC growth emanates from molecular nuclei like $\text{C}_{20}\text{H}_{20}$ and $\text{C}_{15}\text{H}_{20}$.

Many studies explored the aspects of the gas phase chemistry and composition close to the growing diamond surface in a CVD reactor [35]. Most such studies focused on the inter-conversion between small (C_1H_x , C_2H_x , etc) molecular species that are driven by H atom abstraction and addition reactions and control the local densities of CH_3 radicals, which are now generally recognized as the key diamond growth species. The knowledge of larger hydrocarbon species, their relative abundances, stabilities and dependence on process condition is much less developed. However, pertinent points to note are that C_2H_2 is widely recognized as being the most stable (and abundant) hydrocarbon in the “hot” (i.e., near filament) region within a CVD reactor, the proposed seed molecule for IDC growth ($\text{C}_{20}\text{H}_{20}$) can be viewed as a “polymer” of C_2H_2 , and there are many reports of small (but generally as yet uncharacterized) gas phase nanoparticles in the activated hydrocarbon/ H_2 gas mixtures [39].

Finally, careful inspection of the SEM images shown in Fig. 1 shows that, in contrast to the simulated particles, the as-grown “IDCs” and “FSDCs” are not in fact fully symmetric. Such is to be expected, since any realistic picture of FSDC growth under CVD condition starts with the seed nucleus on the substrate surface. Almost by definition, therefore, subsequent growth from the gas phase can only occur on the exposed upper part of the seed nucleus, which is consistent with the cross-sectional image shown in Fig. 1(b).

6 Conclusions

1) The dodecahedrane ($\text{C}_{20}\text{H}_{20}$) molecule is proposed as a nucleus for the growth of IDC, wherein the 20 $\{111\}$ surface planes develop orthogonal to the direction of the original 20 C—H bonds by sequential H abstraction and CH_3 addition reactions.

2) IDC can be pictured as an assembly of isosceles tetrahedra, with each tetrahedron contributing a $\{111\}$ plane to the surface of the IDC and the remainder of the tetrahedral surfaces forming twin planes with neighbouring tetrahedra. The small mismatch (1.44°) between the $\{111\}$ surface dihedral angle of a perfect icosahedron and that of a twinned icosahedron reveals itself via twin planes in the IDC grain.

3) The modelling suggests how the relief of strain induced by this distortion could lead to the formation of defects such as concave pentagonal cavities at vertices and grooves along the grain edges that accord well with those observed experimentally.

4) Similar arguments based on growth from the hexacyclo pentadecane (C₁₅H₂₀) nucleus can also account for the observed formation of star- and rod-shaped FSDCs, and some of their more obvious morphological defects.

Acknowledgements

The authors wish to thank Professor M. N. R. ASHFOLD, Professor J. N. HARVEY, Drs T. B. Scott, O. J. L. FOX, K. O'DONNELL (they all come from University of Bristol), S. J. HENLEY (University of Surrey) and I. HOVLAND for their many and varied contributions to the work.

References

- TORQUATO S, JIAO Y. Dense packings of polyhedra: Platonic and archimedean solids [J]. *Physical Review E*, 2009, 80(4): 041104–21.
- YANG P, KATTAWAR G W, WISCOMBE W J. Effect of particle asphericity on single-scattering parameters: Comparison between Platonic solids and spheres. [J]. *Applied Optics*, 2004, 43(22): 4427–4435.
- ABE E, YAN Y, PENNYCOOK S J. Quasicrystals as cluster aggregates [J]. *Nature Materials*, 2004, 3(11): 759–767.
- SHECHTMAN D, BLECH I, GRATIAS D, CAHN J W. Metallic phase with long-range orientational order and no translational symmetry [J]. *Physical Review Letters*, 1984, 53(20): 1951–1954.
- International Union of Crystallography. Report of the executive committee for 1991 [J]. *Acta Crystallographica A*, 1992, 48: 922–946.
- TALAPIN D V, SHEVCHENKO E V, BODNARCHUK M I, YE X, CHEN J, MURRAY C B. Quasicrystalline order in self-assembled binary nanoparticle superlattices [J]. *Nature*, 2009, 461: 964–967.
- SHECHTMAN D, BLECH I, GRATIAS D, CAHN J W. Metallic phase with long-range orientational order and no translational symmetry [J]. *Physical Review letters*, 1984, 53(20):1951–1954.
- MACI E. The role of aperiodic order in science and technology [J]. *Reports on Progress in Physics*, 2006, 69: 397–441.
- van BLAADEREN A. Materials science: Quasicrystals from nanocrystals [J]. *Nature*, 2009, 461(7266): 892–893.
- MAN W, MEGENS M, STEINHARDT P J, CHAIKIN P M. Experimental measurement of the photonic properties of icosahedral quasicrystals [J]. *Nature*, 2005, 436(18): 993–996.
- HUBERT H, DEVOUARD B, GARVIE L A J, KEEFFE M O, BUSECK P R, PETUSKEY W T, MCMILLAN P F. Icosahedral packing of B12 icosahedra in boron suboxide (B₆O) [J]. *Nature*, 1998, 391(22): 376–378.
- ZHAO Y, KIM Y H, DU M H, ZHANG S B. First-principles prediction of icosahedral quantum dots for tetravalent semiconductors [J]. *Physical Review Letters*, 2004, 93(1): 015502–4.
- YAMAMOTO A, TAKAKURA H. Six-dimensional model of icosahedral Al–Pd–Mn quasicrystals [J]. *Physical Review B*, 2003, 68: 094201–13.
- VAST N, BARONI S, ZERAH G, BESSON J M, POLIAN A, GRIMSDITCH M, CHERVIN J C. Lattice dynamics of icosahedral a-boron under pressure [J]. *Physical Review Letters*, 1997, 78(4): 693–676.
- WANG R M, DMITRIEVA O, FARLE M, DUMPICH G, YE H Q, POPPA H, KILAAS R, KISIELOWSKI C. Layer resolved structural relaxation at the surface of magnetic FePt icosahedral nanoparticles [J]. *Physical Review Letters*, 2008, 100(1): 017205–4.
- SHEVCHENKO V Y, MADISON A E, MACKAY A L. Coherent coexistence of nanodiamonds and carbon onions in icosahedral core-shell particles [J]. *Acta Crystallographica A*, 2007, 63: 172–174.
- KROTO H W, MCKAY K. The formation of quasi-icosahedral spiral shell carbon particles [J]. *Nature*, 1988, 331(28): 328–331.
- ZEGER L, KAXIRAS E. New model for icosahedral carbon clusters and the structure of collapsed fullerite [J]. *Physical Review Letters*, 1993, 70(19): 2920–2923.
- MATSUMOTO S, MATSUI Y. Electron microscopic observation of diamond particles grown from the vapour phase [J]. *Journal of Materials Science*, 1983, 18: 1785–1793.
- SHECHTMAN D. Twin quintuplet surfaces in CVD diamond [J]. *Journal of Materials Science*, 2006, 41(23): 7720–7724.
- WANG W N, FOX N A, DAVIS T J, RICHARDSON D, LYNCH G M, STEEDS J W, LEE J S. Growth and field emission properties of multiply twinned diamond films with quintuplet wedges [J]. *Applied Physics Letters*, 1996, 69(19): 2825–2827.
- BUHLER J, PRIOR Y. Study of morphological behavior of single diamond crystals [J]. *Journal of Crystal Growth*, 2000, 209: 779–788.
- MANI R C, SUNKARA M K. Kinetic faceting of multiply twinned diamond crystals during vapor phase synthesis [J]. *Diamond and Related Materials*, 2003, 12: 324–329.
- SAWADA H, ICHINOSE H. Atomic structure of fivefold twin center in diamond film [J]. *Diamond and Related Materials*, 2005, 14: 109–112.
- YU Z, KARLSSON U, FLODSTROM A. Influence of oxygen and nitrogen on the growth of hot-filament chemical vapor deposited diamond films [J]. *Thin Solid Films*, 1999, 342(1–2): 74–82.
- WEI Q P, ASHFOLD M N R A, YU Z M, MA L. Fabrication of high density, adherent films of five-fold symmetric diamond crystals by hot filament chemical vapour deposition [J]. *Journal of Crystal Growth*, 2011, 336(1): 72–76.
- YU Z, FLODSTROM A. Orientation of (1×1)-surface free energies of crystals [J]. *Surface Science*, 1998, 401(2): 236–247.
- SCHEEL H J, FUKUDA T. *Crystal growth technology* [M]. Chichester, England: John Wiley & Sons Ltd, 2003.
- SCHULMAN J M, VENANZI T, DISCH R L. Theoretical study of dodecahedrane molecule [J]. *Journal of the American Chemical Society*, 1975, 97(19): 5335–5339.
- PAQUETTE L A, BALOGH D W, USHA R, KOUNTZ D, CHRISTOPH G G. Crystal and molecular structure of a pentagonal dodecahedrane [J]. *Science*, 1981, 211(4482): 575–576.
- PAQUETTE L A, TERNANSKY R J, BALOGH D W, KENTGEN G. Total synthesis of dodecahedrane [J]. *Journal of the American Chemical Society*, 1983, 105(16): 5446–5450.
- PAQUETTE L A, MIYAHARA Y, DOECKE C W. Preparatively useful dehydrogenative method for dodecahedrane synthesis [J]. *Journal of the American Chemical Society*, 1986, 108(7): 1716–1718.
- PAQUETTE L A, WEBER J C, KOBAYASHI T. Chemical properties of dodecahedrane. Monofunctionalization reactions [J]. *Journal of the American Chemical Society*, 1988, 110(4): 1303–1304.
- PAQUETTE L A, KOBAYASHI T, KESSELMAYER M A, GALLUCCI J C. Small-ring annulation and ring expansion of the dodecahedrane framework. Homododecahedrane and the 21-homododecahedryl cation [J]. *Journal of Organic Chemistry*, 1989, 54(12): 2921–2930.

- [35] BUTLER J E, MANKELEVICH Y A, CHEESMAN A, MA J, ASHFOLD M N R. Understanding the chemical vapor deposition of diamond: recent progress [J]. *Journal of Physics—Condensed Matter*, 2009, 21(36): 364201–20.
- [36] HAJI-AKBARI A, ENGEL M, KEYS A S, ZHENG X, PETSCHKE R G, PALFFY-MUHORAY P, GLOTZER S C. Disordered, quasicrystalline and crystalline phases of densely packed tetrahedra [J]. *Nature*, 2009, 462: 773–778.
- [37] WILD C, KOIDL P, MILLER-SEBERT W, WALCHER H, KOHL R, HERRES N, LOCHER R, SAMLENSKI R, BRENN R. Chemical vapour deposition and characterization of smooth {100}-faceted diamond films [J]. *Diamond and Related Materials*, 1993, 2(2–4): 158–168.
- [38] SILVA F, BONNIN X, ACHARD J, BRINZA O, MICHAU A, GICQUEL A. Geometric modeling of homoepitaxial CVD diamond growth: I. The {100}{111}{110}{113} system [J]. *Journal of Crystal Growth*, 2008, 310(1): 187–203.
- [39] HWANG N M, LEE D K. Charged nanoparticles in thin film and nanostructure growth by chemical vapour deposition [J]. *Journal of Physics D—Applied Physics*, 2010, 43(48): 483001–38

二十面体金刚石和其他五重对称金刚石晶体的生长机制

魏秋平^{1,2,3}, 马莉^{2,3}, 叶浚⁴, 余志明¹

1. 中南大学 材料科学与工程学院, 长沙 410083;
2. 中南大学 粉末研究国家重点实验室, 长沙 410083;
3. 中南大学 冶金与环境学院, 长沙 410083;
4. 南洋科技大学 材料科学与工程学院, 新加坡 639798

摘要: 采用热丝化学气相沉积(HFCVD)方法制备五重对称金刚石晶体(FSDCs)。利用扫描电子显微镜(SEM)对其表面形貌和缺陷进行观察。从形核-长大的角度出发, 讨论各种五重对称金刚石晶粒的形成机制, 并进行计算机模拟。结果表明: 正十二面体烷($C_{20}H_{20}$)可作为二十面体金刚石晶体(IDC)的晶核, 其 C—H 键垂直于 IDC 的 {111} 表面, 随着活性 H 原子和甲基的不断萃取与结合, $C_{20}H_{20}$ 中 20 个 C—H 键均发展成为与之垂直的 20 个 {111} 表面。正二十面体金刚石晶体(IDC)可以看做是由等腰四面体组装而成, 其中每个四面体给 IDC 表面贡献一个 {111} 晶面, 而四面体的其余晶面与其相邻的四面体形成孪晶面。然而, 完美二十面体 {111} 面的二面角与孪晶结构的二面角存在 1.44° 的差异, 该失配导致了 IDC 的晶格畸变。通过计算模拟讨论晶格失配对 IDC 长大过程中的能量和稳定性的影响, 最终揭示晶格失配所导致的应变如何诱导产生各种缺陷, 如顶点处凹五角形腔的形成, 以及沿晶粒边缘的凹槽。该计算模型能够较好地解释实验中所观察到的晶体形貌。类似推理可进一步用于解释十五烷($C_{15}H_{20}$)作为晶核如何发展成为实验中所观察到的星形和棒形的五重对称结构, 以及一些常见缺陷的形成。

关键词: 金刚石; 五重对称; 二十面体; 十二面体; 缺陷

(Edited by Mu-lan QIN)